Research in Astron. Astrophys. **2013** Vol. **13** No. **11**, 1363–1380
http://www.raa-journal.org *http://www.iop.org/journals/raa*

Research in Astronomy and Astrophysics

Noise reduction methods in the analysis of near infrared lunar occultation light curves for high angular resolution measurements

Tapas Baug and Thyagarajan Chandrasekhar

Physical Research Laboratory, Ahmedabad-380009, India; *tapasb@prl.res.in*

Received 2013 May 1; accepted 2013 June 15

Abstract A lunar occultation (LO) technique in the near-infrared (NIR) provides angular resolution down to milliarcseconds for an occulted source, even with ground-based 1 m class telescopes. LO observations are limited to brighter objects because they require a high signal-to-noise ratio (S/N $\sim$40) for proper extraction of angular diameter values. Hence, methods to improve the S/N ratio by reducing noise using Fourier and wavelet transforms have been explored in this study. A sample of 54 NIR LO light curves observed with the IR camera at Mt Abu Observatory has been used. It is seen that both Fourier and wavelet methods have shown an improvement in S/N compared to the original data. However, the application of wavelet transforms causes a slight smoothing of the fringes and results in a higher value for angular diameter. Fourier transforms which reduce discrete noise frequencies do not distort the fringe. The Fourier transform method seems to be effective in improving the S/N, as well as improving the model fit, particularly in the fainter regime of our sample. These methods also provide a better model fit for brighter sources in some cases, though there may not be a significant improvement in S/N.

Key words: methods: analytical — techniques: high angular resolution — methods: lunar occultation — infrared: stars — stars: late type

1 INTRODUCTION

The lunar occultation (LO) technique in the near-infrared (NIR) is capable of providing high angular resolution information down to 1 mas for occulted stellar sources. It is among the most rapid celestial events with the entire event occurring over just a few hundred milliseconds. The acquisition of LO fringes requires sampling the high speed photometry in the millisecond range. The LO fringes are due to a Fresnel diffraction pattern of the light from the occulted stellar source produced by the sharp edge of the lunar limb. Various effects, like the optical bandwidth (BW) of the filter used, the averaging effect of the telescope aperture, subtraction of sky background and the time response of the detector system, have to be correctly taken into account in order to extract the proper value of angular diameter (in milliarcseconds) for the occulted source. One of the main drawbacks in analysis is the limitation imposed by the signal-to-noise ratio (S/N) of the detected diffraction pattern. A minimal S/N $\sim$40 is usually required to have a good measurement of the angular diameter. An LO light curve with a very high S/N ($>$100) in the fringe region can also be investigated for signatures

of circumstellar material surrounding a star. Detecting finer structural information about the inner dust shell associated with sources, for example WR 104 and IRC +10216 (Mondal & Chandrasekhar 2002; Chandrasekhar & Mondal 2001), is only possible in light curves with relatively high S/N. However, the fast sampling and good S/N are conflicting requirements and set a limit on the magnitude of observable sources using the LO technique. With our current detector system (NICMOS IR Camera), sources up to $m_K \sim 5.0$ are observable under good sky conditions. The earlier system (a single element InSb photometer) could only reach up to $m_K \sim 3.0$ but with good sampling down to 1 ms. In this paper, attempts have been made to explore different noise detection and reduction techniques to reduce the noise content in the LO light curves and thereby enhance the S/N.

LO observations are carried out in the NIR K-band (2.2 μm) to reduce scattering from the lunar background. Compared to the K-band, the lunar background is higher in two other NIR bands, namely J (1.25 μm) and H (1.65 μm) as well as visible bands. Also LO in the K-band is capable of providing information about the true photosphere at high angular resolution as well as the circumstellar shell, if one is present. It is difficult to acquire information about the shell in the other NIR bands, J and H. This study scrutinizes late-type giants since they are brighter in the K-band compared to visible bands. The LO light curve in NIR (2.2 μm) suffers from contributions of noise due to both source and background. Scintillation noise is more prominent in the case of brighter sources. Scintillation noise also depends on altitude above the horizon; at lower altitudes the scintillation noise is a more serious problem. Hence, the recorded light curves show a low frequency variation in the signal level when the star is available. In Figure 1, which is the LO light curve of SAO 118044 ($m_K \sim$0.5), low frequency variation of the signal level can be noticed before occultation. Another definite cause of noise in the astronomical observations of incoherent sources is photon noise from the source, which arises due to intrinsic natural variation of the emitted photon flux. This creates a high frequency fluctuation in the signal level of the observed LO light curve. It can be noticed that in the first half of the light curve, high frequency fluctuations created due to stellar photon noise are modulated by low frequency scintillation noise. By contrast, the second half of the light curve is mainly dominated by photon noise from the background because the source is absent there. The corresponding power spectrum representing the two parts of the light curve of SAO 118044 is shown in Figure 2. The first part of the light curve is dominated by low frequency noise, which is mainly scintillation noise. The second half of the light curve is dominated by specific noise frequencies.

The S/N of NIR observations is usually limited by sky noise due to scattered moonlight (which varies with lunar phase), airglow intensity (which varies), and also thermal contribution from telescope optics, especially when a broad K-band filter is used. From our observed light curves we found that the dominant component of noise changes from source to background at K-magnitude of about 3.3 under good sky conditions and at good altitudes for observations ($>40^\circ$). Another significant contribution of noise in the light curves comes from electrical line pick-up (50 Hz) and a 31 Hz noise frequency from electronics in the detector. Although it was ascertained to originate from electronics in the detector, attempts to eliminate this noise from the hardware were not successful.

A Fourier transform (FT) is capable of detecting independent, non-evolving periodicities in stationary signals. FTs have been extensively used in different aspects of astrophysics, particularly for identifying and processing stationary time series data. The application of Fourier analysis to identify low frequency correlated noise in binary pulsar data can be found in Kopeikin & Potapov (2004). In a recent paper, Kashlinsky et al. (2012) applied FTs for measurements of cosmic infrared background fluctuations using *SPITZER* data. The power spectra of source subtracted fields were examined to eliminate or identify different noise components.

Recently, the wavelet transform (WT) has been widely implemented for analyzing oscillations, periodicities, as well as a sudden change in the observed signal. The decomposition of time series data into signal-like and noise-like components can be found in Polygiannakis et al. (2003). They applied it to a sunspot index to search for periodicities in the solar cycle other than 11 yr. In a recent paper, Adamakis et al. (2011) used the WT to analyze a long term optical light curve covering about

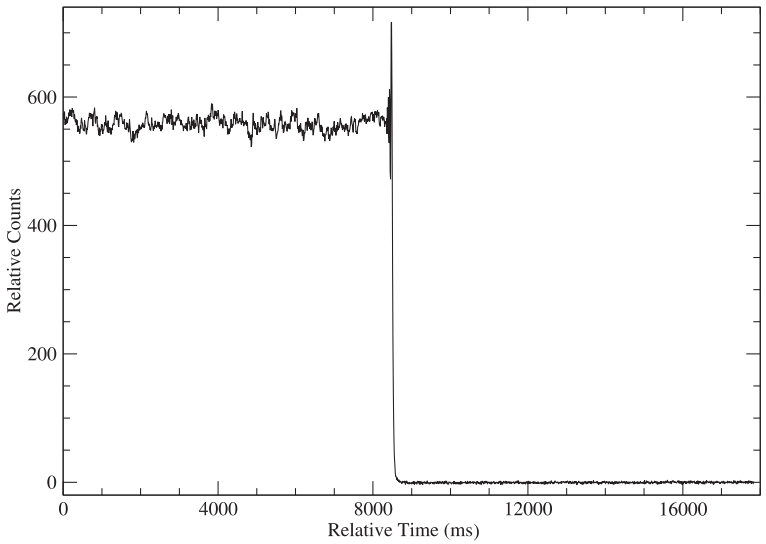

Fig. 1 The light curve of one of the brightest sources, SAO 118044 ($m_K = 0.49$), in our sample shows a different noise pattern before and after the occultation. The first part of the light curve (before the event) is dominated by source photon noise and low frequency scintillation noise. However, the second part of the light curve (after the event) is purely dominated by background noise.

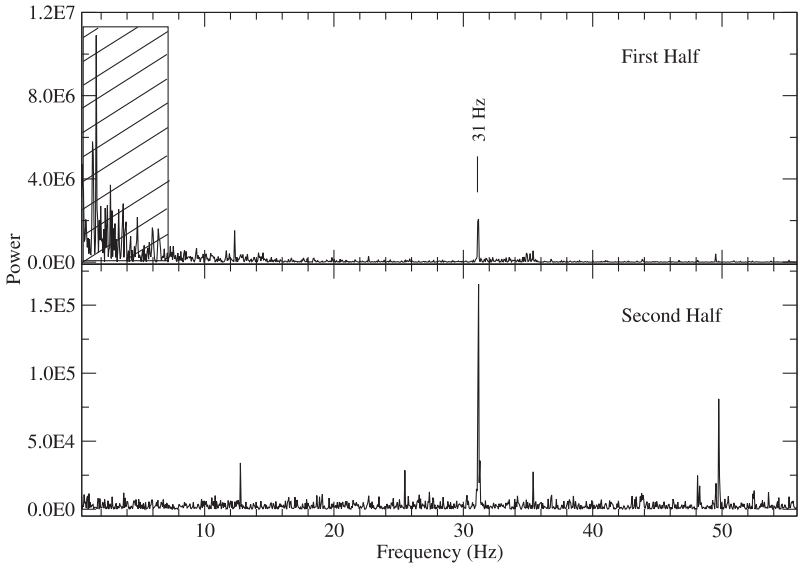

Fig. 2 The power spectrum of the LO light curve of SAO 118044 shown in Fig. 1. Note that different scales have been used for the Y-axis in the two halves. The upper panel shows the power spectrum of the first half of the light curve (before occultation) and the lower panel shows the power spectrum of the second half. The first half of the light curve is dominated by scintillation and source photon noise. There are many low frequency components that can be seen inside the shaded box. In the second half these components are absent. The noise at several discrete frequencies like 31 Hz and 50 Hz with sub-harmonics are present in both halves of the light curve.

76 yr for the nova RS Ophiuchi. From the wavelet power, they identified a pre-outburst signature up to 450 d before the event. This indicates the potential of having an early warning for future outbursts. The WT has also been used in the analysis of LO data. In 2008, Fors et al. used a WT to compute the initial guess of the model parameters while they were analyzing a large data set.

In this paper we have implemented methods to improve the S/N of observed LO light curves by reducing noise content from the observed LO light curves. The noise reduction methods are applied to a sample of 54 light curves with up to $m_K \sim 5.0$ obtained using the NICMOS IR camera attached to the Mt. Abu telescope. Observational details are given in Table 1. The sources in the table are arranged in increasing order of RA. The first column of the table is the designation of the sources, while the second and third columns are date of observations and J2000.0 coordinates respectively. The fourth column represents the NIR K-magnitude of the source as given in the 2MASS catalog (Cutri et al. 2003). The fifth column represents the spectral type of the source collected from the SIMBAD database. Finally, the sixth and seventh columns respectively correspond to the elevation of the source above the horizon and lunar phase (days after the new moon) during the observations.

2 OBSERVATIONS

A total of 54 occultation light curves have been used in the analysis. All the light curves are observed in the NIR broad-K-band (2.2 μm/BW 0.4 μm), except three. Three bright sources are observed in the narrow CO-band (2.37 μm/BW 0.1 μm) to avoid the effect of saturation and they are marked as † in Table 1. All the LO light curves are observed using the NICMOS IR camera attached to the 1.2 m telescope at Mt Abu Observatory (Lat: 24°39′10″, Long: 72°46′47″ E, Alt: 1680 m), India. The NICMOS camera was used in the imaging sub-array mode with size 10×10 pixels ($5'' \times 5''$ on the sky) to sample the events as rapidly as possible. The operational mode for the sub-array of the NICMOS camera was first used for LO observations towards the Galactic center on 2007 September 19 (Chandrasekhar & Baug 2010). Typically an observing run in the sub-array mode consists of initiating the data acquisition procedure for recording 4800 sub-frames about 20 s before the predicted time of the event. About 15 s after the predicted event time, the telescope is rapidly switched to a nearby sky to record sky frames. The star becomes "visible" only in the frames after sky subtraction is performed due to the high level of background in K-band. Sky subtracted sub-frames are used to derive the light curve. All but one source in this sample were observed in the 10×10 pixel mode. With an integration and a reset time of 3 ms each, it provides a sampling time of 8.926 ms. The source IRC +20177 was observed in the 20×20 pixel mode, to accommodate its visual binary component in the sub-array. It had a sampling time of 14 ms.

3 ANALYSIS

3.1 Fourier Denoising Method

Any stationary signal can be decomposed into its component frequencies using FTs. It converts the signal from the time-amplitude domain to the frequency-power domain. However, one of the drawbacks of the FT process is that the time information of the signal is lost in the frequency domain; which means, the specific time of occurrence of any particular frequency is completely lost. In the present case most of the light curves are sampled at an interval of 8.926 ms and the corresponding *Nyquist* frequency is 56.0 Hz. In our LO light curves, specific well-identified noise frequencies like 31 Hz and 50 Hz and their sub-harmonics are present. Hence, it is useful to apply FTs to remove these frequencies. The Fourier denoising (FD) method is applied to our sample consisting of 54 observed light curves (Table 1). A MATLAB script written by us was used in the analysis. A standard set of 4096 data points for each light curve was used for all the transformations.

The very initial and fundamental problem in applying the FT to LO data is related to the FT itself. The FT of a step function (Fig. 3) has rapidly decreasing power ($\propto \frac{1}{\mathrm{freq}^2}$) from low frequencies to

Table 1 Details of observations of LO events at the Mt. Abu Observatory, observed in the near infrared K-band (2.2 μm/BW 0.4 μm)

Source	Date of Observations	Coordinates (J2000.0)	m_K (2MASS)	Sp. type	El (°)	Lunar Phase
SAO 109252	2011 Jan 11	00 31 37.360 +09 09 40.26	3.74	K2	57.8	7.22
SAO 92697	2009 Nov 29	01 55 31.157 +17 11 21.72	2.03	M6	70.9	12.83
SAO 92755[a]	2009 Nov 29	02 01 30.386 +17 57 13.79	2.50	M...	47.0	13.02
SAO 92755[b]	2010 Jan 23	02 01 30.386 +17 57 13.79	2.50	M...	82.9	8.25
IRC +20037	2010 Jan 23	02 03 42.621 +18 15 11.69	2.90	K4III	61.4	8.33
UY Ari	2011 Jan 13	02 05 49.064 +17 29 34.53	3.69	M5	80.4	9.22
AU Ari	2011 Jan 13	02 08 56.711 +17 34 45.95	3.68	M0	52.0	9.31
SAO 75669	2011 Jan 14	02 58 48.237 +20 35 39.75	3.35	M0	78.1	10.26
UZ Ari[a]	2009 Nov 30	03 01 34.722 +21 48 12.19	1.25	M8	40.8	14.08
UZ Ari[b]	2010 Jan 24	03 01 34.722 +21 48 12.19	1.25	M8	46.4	9.41
SAO 75706	2011 Jan 14	03 03 03.525 +21 10 23.84	3.71	M0	34.0	10.40
IRAS 03333+2359	2009 Jan 07	03 36 22.250 +24 09 27.75	5.07	–	55.9	10.03
IRC +20066	2011 Jan 15	03 53 54.698 +23 07 47.36	2.60	M...	87.3	11.27
NSV 1406	2011 Jan 15	03 54 43.086 +23 19 12.13	2.93	M4	73.9	11.31
SAO 76350	2010 Jan 25	03 57 26.391 +24 27 43.05	3.20	K0	85.2	10.33
V1134 Tau	2009 Mar 03	04 04 11.955 +25 23 56.61	3.84	M0	43.3	6.60
SAO 76450	2010 Jan 25	04 06 04.684 +24 43 55.51	3.06	S3/3	21.2	10.54
IRAS 04320+2519[a]	2009 Dec 29	04 35 05.617 +25 26 00.46	4.30	–	46.0	13.35
IRAS 04320+2519[b]	2010 Feb 22	04 35 05.617 +25 26 00.46	4.30	–	78.5	8.48
C* 3246	2010 Jan 26	04 57 20.878 +25 37 44.35	3.58	C	60.0	11.26
IRAS 05013+2704	2009 Mar 04	05 04 30.698 +27 08 26.29	4.12	–	74.1	7.54
SAO 76952	2011 Mar 12	05 05 12.039 +23 47 56.26	4.70	K0	44.3	7.81
SAO 76965	2009 Mar 04	05 07 05.162 +26 59 45.30	4.40	F5V	57.8	7.59
IRAS 05212+2655	2009 Feb 05	05 24 19.176 +26 58 22.04	3.74	–	75.9	10.27
IRAS 05232+2400	2011 Feb 13	05 26 16.887 +24 02 58.82	3.94	–	72.2	10.58
SAO 77229	2009 Feb 05	05 31 56.397 +26 41 05.94	3.87	K2	44.0	10.46
SAO 77271	2009 Dec 30	05 34 51.086 +25 53 03.80	3.27	K7	75.6	14.21
SAO 77357	2010 Feb 23	05 39 32.010 +25 18 45.07	4.39	M0	69.8	9.55
SAO 77474	2010 Feb 23	05 44 07.749 +25 22 25.59	4.14	K5	38.6	9.65
HD 249571	2011 Mar 13	05 57 38.274 +23 33 28.98	4.50	M0III	84.7	8.69
SAO 77792	2011 Jan 17	05 58 38.163 +23 39 57.94	2.97	M2	58.5	13.44
IRAS 05551+2305	2011 Mar 13	05 58 10.549 +23 06 20.76	4.18	–	88.0	8.71
BI Gem	2010 Jan 27	06 05 49.697 +25 14 41.56	3.17	M6	71.9	12.34
IRC +30140	2009 Mar 05	06 09 20.095 +26 31 42.25	2.70	M1	88.1	8.54
TU Gem	2009 Jan 09	06 10 53.107 +26 00 53.32	0.82	C	18.5	12.46
BD+26 1131	2009 Mar 05	06 12 22.576 +26 20 03.86	4.06	M3IIIe...	65.1	8.61
IRAS 06165+2431	2010 Mar 23	06 19 37.503 +24 30 25.59	4.87	–	80.1	7.71
IRAS 06395+2409	2010 Feb 24	06 42 35.253 +24 06 41.56	3.66	–	87.7	10.54
IRC +20177	2010 Jan 28	07 20 07.367 +21 58 56.12	2.56	F0IV	51.2	13.57
IRC +20186	2009 Feb 07	07 40 58.525 +23 01 06.75	2.18	K5III	84.4	12.39
VV Cnc	2010 Jan 29	08 11 16.298 +19 08 54.59	0.94	M5	20.7	14.27
CW Cnc†	2010 Apr 22	09 08 26.526 +13 13 13.64	0.11	M6	18.3	8.28
6 Leo	2011 Apr 13	09 31 57.591 +09 42 57.04	1.98	K2.5IIIb	42.9	10.16
IRC +10210	2010 May 20	09 41 09.022 +09 53 32.11	2.50	A5V+...	64.5	6.56
SAO 118044	2010 Apr 23	10 00 12.812 +08 02 39.13	0.49	M2III	45.3	9.23
IRC +00202	2009 May 31	11 06 02.226 +01 12 38.34	2.59	M...	38.5	7.19
SAO 157613	2009 May 06	12 56 43.052 –11 56 37.14	3.24	K5	52.8	11.59
CW Oph	2011 May 18	16 55 39.099 –23 52 25.91	2.65	M7:	37.5	15.50
RT Cap	2008 Dec 02	20 17 06.516 –21 19 04.30	0.31	C	42.3	4.70
RS Cap†	2008 Dec 03	21 07 15.428 –16 25 21.50	-0.22	M6-7III	45.8	5.82
IRC –10564	2008 Nov 06	21 30 37.105 –14 10 18.85	2.22	M4III:	16.7	8.78
SAO 145698	2010 Dec 11	21 50 35.452 –08 58 57.26	3.80	K0	52.7	5.80
SAO 145992	2008 Dec 07	22 16 52.574 –09 02 24.45	3.22	K3III:	35.7	9.75
TX Psc†	2011 Nov 06	23 46 23.520 +03 29 12.15	-0.51	C	68.9	10.83

† Sources were observed in the narrow CO-band (2.37 μm; BW 0.1 μm). The sources which have been observed twice are marked with superscripts a and b in the column. ":" There was an inaccuracy in the temperature or luminosity class.

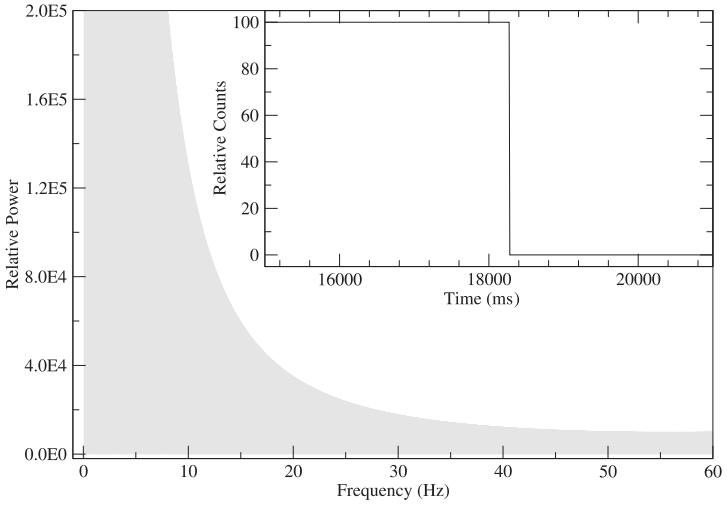

Fig. 3 A step function (inset) and its power spectrum. The power spectrum shows rapidly decreasing power towards higher frequencies.

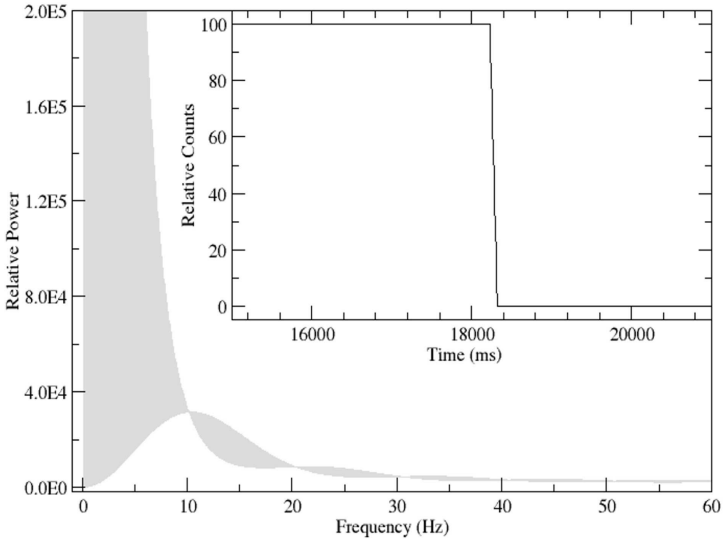

Fig. 4 A step function with a slope (inset) and its power spectrum. The power spectrum shows an oscillatory behavior along with the rapidly decreasing power.

higher frequencies, but a step function with a slope shows a similar pattern with an additional low frequency modulation associated with it (Fig. 4). The signal level in LO light curves also changes before and after the occultation, like a step function with a slope, and shows a similar characteristic in the Fourier domain (Fig. 5). The high frequency oscillations in the power spectrum arise due to the step function-like nature of the light curve. The low frequency modulation in the power spectrum is obtained from the decline of the light curve after occultation. The flatter the slope in the light curve is,

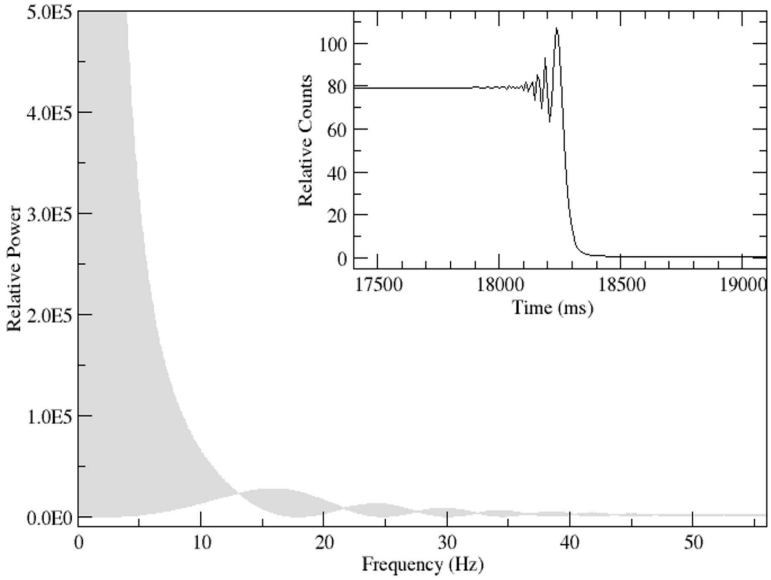

Fig. 5 The power spectrum of a model LO light curve of a 2 mas source (inset) is similar to that of the step function with a slope, as shown in Fig. 4.

the higher the frequency of the second type of variation will be. This implies that even well-identified noise frequencies are not easy to completely remove, as a part of the resulting power is always contributing to define the shape of the light curve itself. The effect is higher in the low frequency regime ($<$10 Hz) of the power spectrum. Frequencies greater than 10 Hz can be completely removed from light curves without creating any significant distortion. A schematic diagram of the denoising method is shown in Figure 6 (left).

The faintest object in our sample, IRAS 03333+2359, has also shown a slight improvement after the application of the FD method (Fig. 7). The S/N increased from 21 to 24. The corresponding power spectrum of the light curve is also shown in Figure 8 and components that have been removed are marked in it. A few well-identified noise frequencies, like a 50 Hz power line pick-up, its sub-harmonics, and 31 Hz, etc, are seen in the spectrum. It also occasionally happens that the fringe frequency almost matches the low frequency fluctuations in the signal. It can be seen that the 31 Hz noise frequency is present in almost all light curves and it contributes the dominate source of power in many sources (mainly fainter objects). The main goals in applying the FD method are to remove these two (31 Hz and 50 Hz) well-identified noise frequencies and their sub-harmonics. However, in a few cases some other frequencies, that had dominate power, have also been removed from the light curves but those frequencies are higher than 10 Hz. A MATLAB programming script was written and used to implement this method. The method was applied to all 54 sources listed in Table 1. The light curve of the source SAO 77271 showed the best improvement in S/N after application of the FD method (Fig. 9). The power spectrum of the corresponding light curve is also shown in Figure 10. The frequencies that were removed are marked in the power spectrum. Removal of those frequencies enhanced the S/N of the light curve from 32 to 55.

A histogram plot of source vs. S/N for both observed (hereafter called Raw) (upper) and FD (middle) is displayed in Figure 11. It is seen that the FD method has improved the S/N, but not dramatically. A few light curves with lower S/N have increased their S/N $>$40.

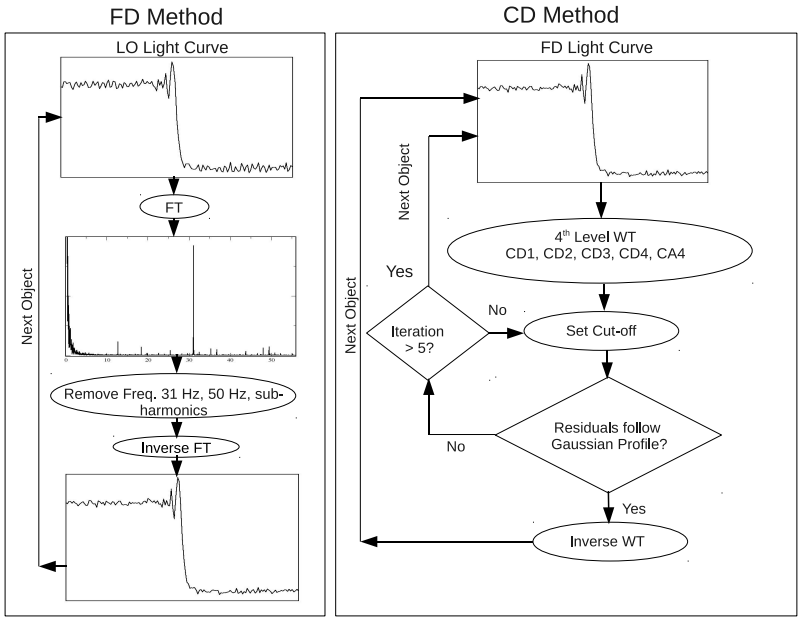

Fig. 6 The schematic diagram of the Fourier (*left*) and Combination (Fourier + Wavelet) denoising methods (*right*).

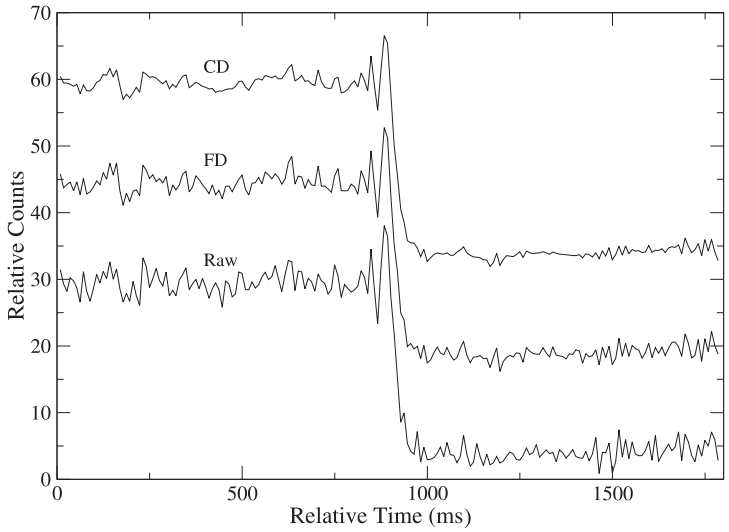

Fig. 7 Raw, Fourier and a combination of Fourier and wavelet denoised light curves of IRAS 03333+2359. The Fourier and combined denoised light curves are shifted upward by 15 and 30 counts respectively to avoid overlap and for clarity. S/N has improved from 21 (Raw) to 24 (FD) which is further improved to 32 after the application of the CD method.

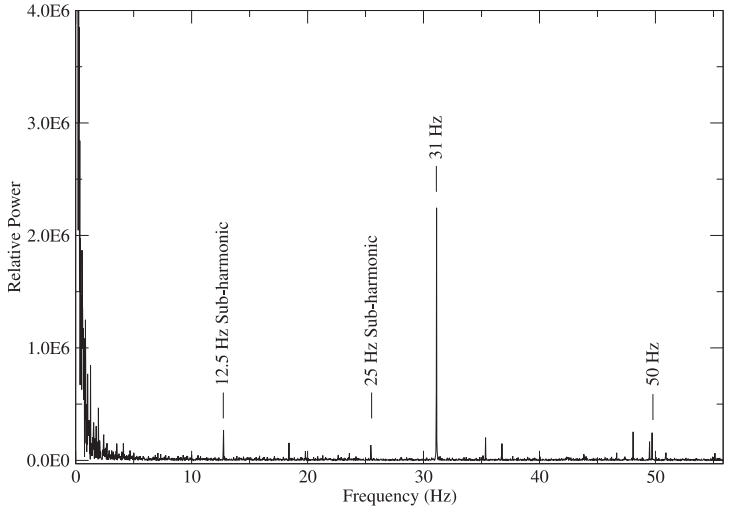

Fig. 8 The power spectrum of the Raw light curve of IRAS 03333+2359. The frequencies, marked in the spectrum, are removed from the light curve by applying the FD method.

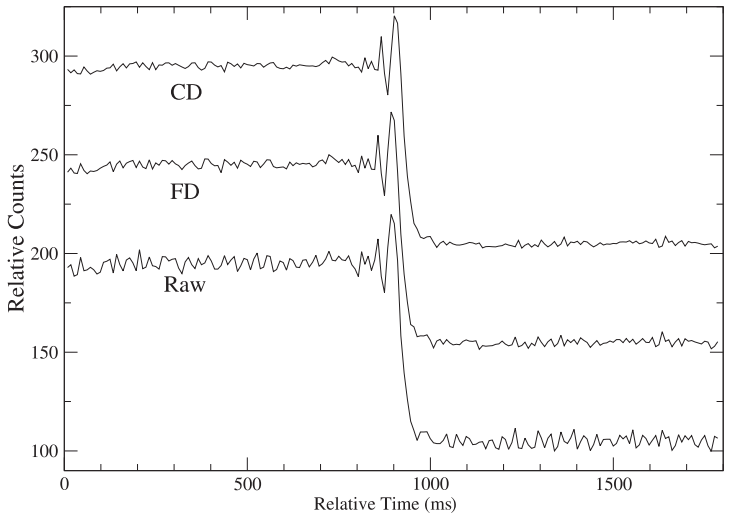

Fig. 9 Raw, Fourier and a combination of Fourier and wavelet denoised light curves of SAO 77271. The Fourier and combined denoised light curves are shifted upward by 50 and 100 counts to avoid overlap and for clarity. The denoised light curves can be clearly seen to have less noise than the observed (Raw) data. S/N has improved from 32 (Raw) to 55 (FD), which has also improved further to 74 (CD).

With the help of FTs, only a few specific noise frequencies have been removed. Fluctuations for a limited period may also be present in the light curves, which contain lesser power in the frequency-power domain. Hence, it is difficult to identify and remove them individually. Handling these noisy light curves motivated us to investigate the use of WTs.

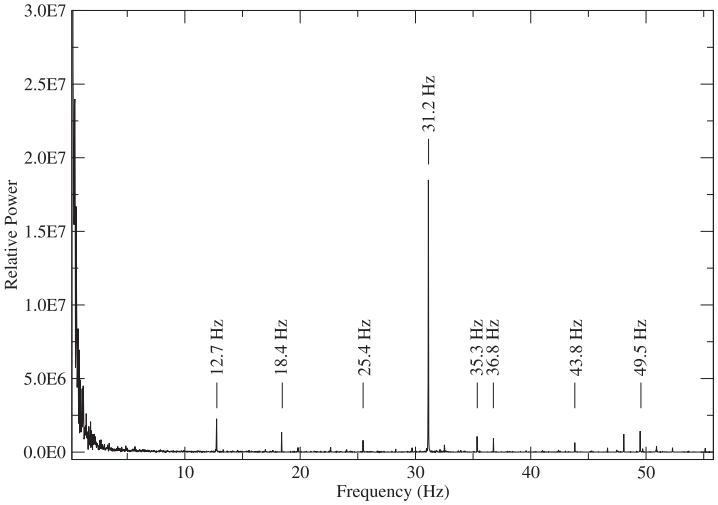

Fig. 10 The power spectrum of the Raw light curve of SAO 77271. The frequencies, marked in the spectrum, are removed from the light curve by applying the FD method.

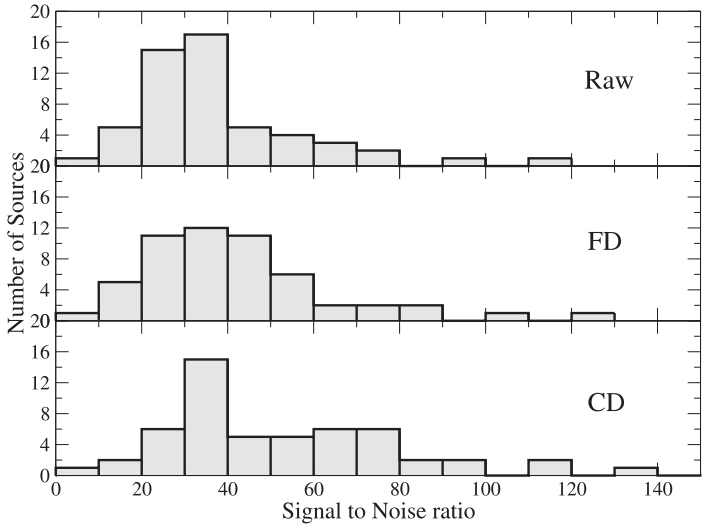

Fig. 11 The histogram shows that nine sources have increased S/N >40 after the application of the FT method. The number further increased by 5 after the application of WT in the CD method.

4 WT APPLICATION ON LO DATA

The MATLAB wavelet tools and also scripts written by us have been used to perform the noise reduction of the LO light curves using wavelets. Many mathematical forms of wavelets have been presented in the literature. Generating a user defined wavelet filter is also possible, subject to certain conditions being satisfied. To select a suitable wavelet to be used in the decomposition of LO data,

a sample of 15 different wavelets from a few light curves has been analyzed. It was found that two specific wavelets among them, namely coiflet 4 and symlet 20, are suitable for filtering the LO light curves.

The application of WTs to a signal first decomposes it into several detail coefficients and one average coefficient according to the level of decomposition. For example, after 3rd level decomposition it produces three detail coefficients, namely, *cd1*, *cd2* and *cd3* and one average coefficient *ca3*, where *cd1* corresponds to coefficients with the highest frequencies. Photon noise contributes to the two highest frequency coefficients. The contribution from the scintillation creates low frequency variations in the light curve and hence, they appear in the higher level detail coefficients.

To remove the high frequency noise from the signal, cut-off limits for each component are implemented manually. Two cut-off modes are available in MATLAB: (1) Soft-cutoff and (2) Hard-cutoff. In Soft-cutoff a certain amount of amplitude is deducted from all the coefficients, while in the case of Hard-cutoff, amplitudes above the given cutoff value are clipped. Here, Soft-cutoff has been used for noise removal of the light curves. In light curves obtained from LO, mainly the highest frequency coefficients are removed because they represent Gaussian noise. Hence, the condition is imposed that their residuals (Raw − denoised) should follow a Gaussian distribution with zero mean. A schematic diagram of the denoising method is shown in Figure 6 (right).

Wavelet denoising has been applied to all 54 LO light curves. Though significant improvement was obtained in the S/N by using the WT method, it is found that pure noise frequencies like 31 Hz and 50 Hz are also present with significant power in the wavelet denoised light curves. The wavelet denoising method also has an averaging effect, because it removes the detail coefficients at a certain cutoff. The reduction of high frequency fluctuations from the average base-level would always lead to a smoothing effect. The application of WTs on LO light curves acts as a running average and finally smooths the observed light curves. In the model fit, the averaged fringes are fit to higher angular diameter values describing a uniform disk (UD) than the source originally represents.

Considering these issues, it was decided to use a combination of both methods. First, FD is carried out to remove those well-identified specific noise frequencies. Then the WT method was applied in a similar manner as explained above. The WT method was executed after the application of FD to put minimum cut-offs on WT coefficients. This was because the averaging effect depends on the cut-off value. Hence, the combination of Fourier and the wavelet denoising (CD) method has been applied to all 54 LO light curves by setting the cut-off limit manually. Here we also imposed the same condition that residuals (Raw − denoised) should follow a Gaussian distribution with zero mean.

5 RESULTS & DISCUSSION

The result of the applied methods has two implications: (1) the improvement in the S/N of the light curves and (2) improvement in the model fits for possible determination of angular diameter. We first discuss enhancements in S/N using the two methods, namely FD and CD. The numerical details before and after the application of denoising methods are listed in Table 2. The table here is arranged in order of increasing RA. The first column in the table lists the source designations and the second column is the apparent K-magnitude as given in the 2MASS catalog. The S/N values of the Raw and denoised light curves using FD and CD methods are listed in the next three columns of the table, respectively. The descriptions of the other columns are listed in Section 5.2.

5.1 Improvement in S/N after Denoising Methods

5.1.1 S/N after the FD method

The improvement in the S/N using the FD method is graphically shown in the histogram plot in Figure 11. It shows that 9 out of 38 sources have improved their S/N beyond 40 after application of

Table 2 Numerical Details of Raw, FD and CD Light Curves

Source	m_K	S/N			SD_{fringe}			SD_{total}			SD_{ratio}		
		Raw	FD	CD	Raw	FD	CD	Raw	FD	CD	Raw	FD	CD
(1)	(2)	(3)	(4)	(5)	(6)	(7)	(8)	(9)	(10)	(11)	(12)	(13)	(14)
SAO 109252	3.74	31	**35**	**53**	0.64	0.52	0.45	0.66	0.59	0.42	0.97	0.87	1.06
SAO 92697	2.03	47	**52**	**62**	0.92	0.81	0.71	1.02	0.89	0.71	0.90	0.91	0.99
SAO 92755[a]	2.50	28	30	**31**	1.25	1.51	1.43	1.80	1.78	1.68	0.70	0.85	0.85
SAO 92755[b]	2.50	09	09	09	–	–	–	–	–	–	–	–	–
IRC +20037	2.90	34	35	**40**	1.52	1.51	1.38	1.89	1.84	1.61	0.80	0.82	0.86
UY Ari	3.69	37	**41**	**70**	0.90	0.84	0.68	0.74	0.67	0.45	1.22	1.26	1.53
AU Ari	3.68	24	25	**34**	0.97	0.89	0.83	0.89	0.83	0.60	1.09	1.08	1.38
SAO 75669	3.35	26	**30**	**45**	0.83	0.65	0.56	0.94	0.83	0.52	0.88	0.79	1.08
UZ Ari[a]	1.25	42	42	**46**	6.67	7.08	6.83	4.88	4.88	4.52	1.37	1.45	1.51
UZ Ari[b]	1.25	77	**83**	**95**	2.22	2.09	1.92	1.80	1.73	1.56	1.24	1.21	1.24
SAO 75706	3.71	18	19	**23**	0.84	0.86	0.82	0.92	0.84	0.67	0.91	1.03	1.22
IRAS 03333+2359	5.07	21	**24**	**32**	0.67	0.53	0.41	0.71	0.58	0.41	0.94	0.90	0.98
IRC +20066	2.60	65	**75**	**119**	1.05	1.01	1.05	0.98	0.88	0.68	1.08	1.15	1.53
NSV 1406	2.93	26	26	**30**	1.22	1.08	1.00	1.16	1.08	0.89	1.05	1.00	1.12
SAO 76350	3.20	66	**69**	**96**	0.90	0.86	0.87	0.91	0.84	0.68	0.99	1.02	1.28
V1134 Tau	3.84	40	40	**54**	1.03	1.00	0.88	0.95	0.91	0.70	1.09	1.10	1.26
SAO 76450	3.06	21	22	**27**	1.16	1.16	1.08	1.06	1.02	0.83	1.10	1.14	1.30
IRAS 04320+2519	4.30	18	19	**24**	0.94	0.88	0.75	0.89	0.81	0.66	1.05	1.09	1.12
IRAS 04320+2519	4.30	11	12	**14**	1.44	1.37	1.21	1.15	1.08	0.89	1.25	1.27	1.36
C* 3246	3.58	44	**59**	**86**	0.87	0.67	0.55	0.78	0.65	0.47	1.11	1.03	1.17
IRAS 05013+2704	4.12	35	**41**	**62**	0.71	0.64	0.55	0.69	0.61	0.42	1.03	1.05	1.32
SAO 76952	4.70	17	19	**27**	0.81	0.71	0.60	0.93	0.82	0.61	0.87	0.86	0.98
SAO 76965	4.40	28	**31**	**39**	0.66	0.57	0.49	0.67	0.58	0.45	0.99	0.98	1.08
IRAS 05212+2655	3.74	26	28	**31**	1.81	1.68	1.60	1.48	1.38	1.25	1.22	1.22	1.28
IRAS 05232+2400	3.94	33	34	**40**	1.91	1.94	1.76	1.64	1.60	1.46	1.17	1.21	1.20
SAO 77229	3.87	32	**38**	**49**	0.96	0.90	0.87	1.00	0.86	0.67	0.96	1.05	1.30
SAO 77271	3.27	32	**55**	**74**	1.35	0.90	0.86	1.42	0.85	0.68	0.95	1.06	1.25
SAO 77357	4.39	22	27	**40**	0.67	0.55	0.48	0.60	0.52	0.36	1.11	1.06	1.34
SAO 77474	4.14	22	**25**	**35**	0.64	0.62	0.54	0.73	0.67	0.50	0.88	0.94	1.08
HD 249571	4.50	26	**31**	**37**	0.73	0.58	0.51	0.84	0.74	0.59	0.88	0.78	0.87
SAO 77792	2.97	40	**45**	**62**	1.36	1.22	1.11	1.03	0.92	0.73	1.32	1.33	1.52
IRAS 05551+2305	4.18	44	**47**	**70**	0.96	0.85	0.84	0.85	0.82	0.61	1.13	1.03	1.36
BI Gem	3.17	52	**64**	**89**	0.74	0.66	0.62	0.81	0.65	0.50	0.91	1.01	1.24
IRC +30140	2.70	100	**107**	**169**	1.07	0.91	0.94	0.87	0.77	0.53	1.22	1.19	1.78
TU Gem	0.82	32	33	**38**	–	–	–	–	–	–	–	–	–
BD+26 1131	4.06	38	**46**	**68**	0.78	0.57	0.50	0.77	0.66	0.45	1.02	0.87	1.11
IRAS 06165+2431	4.87	20	**23**	**30**	0.63	0.55	0.47	0.64	0.56	0.45	0.97	0.98	1.06
IRAS 06395+2409	3.66	42	**49**	**77**	0.86	0.73	0.60	0.78	0.68	0.46	1.10	1.07	1.29
IRC +20177	2.56	30	**41**	**50**	–	–	–	–	–	–	–	–	–
IRC +20186	2.18	35	35	**39**	4.76	4.69	5.06	3.68	3.71	3.61	1.30	1.26	1.40
VV Cnc	0.94	32	32	**37**	–	–	–	–	–	–	–	–	–
CW Cnc	0.11	19	19	19	7.43	8.08	7.92	5.49	5.86	5.67	1.35	1.38	1.40
6 Leo	1.98	54	55	**63**	5.31	5.34	5.24	4.16	4.10	3.83	1.29	1.30	1.37
IRC +10210	2.50	38	**44**	**57**	1.12	1.08	1.00	1.03	0.91	0.72	1.09	1.18	1.39
SAO 118044	0.49	119	**122**	**138**	2.48	2.44	2.37	2.07	2.03	1.87	1.20	1.20	1.27
IRC +00202	2.59	53	**56**	**77**	0.87	0.82	0.64	0.78	0.70	0.54	1.12	1.17	1.19
SAO 157613	3.24	36	**44**	**72**	0.67	0.65	0.67	0.75	0.66	0.52	0.89	0.99	1.29
CW Oph	2.65	27	**33**	**39**	1.44	1.16	0.98	1.54	1.29	1.10	0.93	0.90	0.90
RT Cap	0.31	38	38	39	11.16	11.27	10.87	9.76	9.79	9.47	1.14	1.15	1.15
RS Cap	-0.22	51	53	**59**	4.25	3.96	3.86	3.55	3.48	3.33	1.20	1.14	1.16
IRC -10564	2.22	24	26	26	2.78	2.77	2.72	2.81	2.79	2.76	0.99	0.99	0.98
SAO 145698	3.80	36	38	**59**	0.58	0.54	0.44	0.59	0.54	0.36	0.99	1.00	1.20
SAO 145992	3.22	80	**86**	**119**	0.87	0.85	0.77	0.96	0.91	0.75	0.91	0.93	1.04
TX Psc	-0.51	63	**73**	**77**	1.53	1.19	0.90	1.29	1.03	0.83	1.18	1.15	1.09

Notes: the sources which have been observed twice are marked with superscripts a and b in the column.

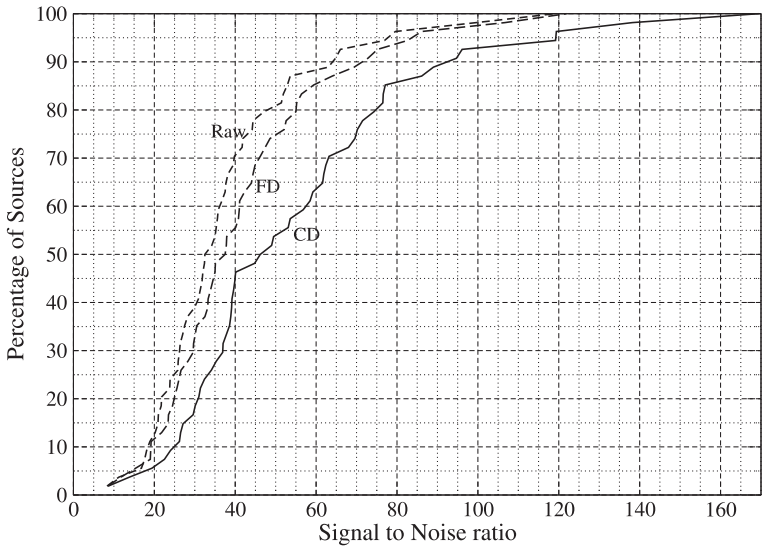

Fig. 12 *Short dashed line* is the cumulative distribution plot of Raw light curves. It has been shifted towards right hand-side after the application of denoising methods, namely FD (*long dashed line*) and CD (*solid line*). For example before application of the denoising method, 70% sources had S/N<40. After the application of FD method, only 56% of the sources have S/N<40 and it has further decreased to 45% after application of WT in CD method.

the FD method, which implies that a 24% improvement has been obtained. A different cumulative representation of the same result is shown in Figure 12. Here, the X-axis corresponds to the S/N of the light curves and the Y-axis represents the percentage of sources below any specific S/N. For example, the short dashed line, representing Raw light curves, shows that 70% of the sources have S/N below 40. It reduces to 56% after application of the FD method (long dashed line).

The sources which show significant improvement in S/N are marked in bold in column 4 of Table 2. It can be noticed that a total of 29 out of 54 sources (more than 50%) show significant ($\geq 3\sigma$) improvement in S/N using the FD method. The remaining 25 sources did not show any improvement in their S/N. Out of these 25 sources, 14 are brighter than m_K ~3.0. Noise in these light curves is dominated by low frequency ($<$ 5 Hz) noise. However, the main noise components removed in the FD method are 50 Hz, its sub-harmonics (25 Hz and 12.5 Hz) and 31 Hz. The removal of low frequency noise (mainly due to scintillation) is difficult as it is not at a single frequency but rises to 5 Hz (see Fig. 2) with varying power. Complete removal of the low frequency component leads to a distortion of LO fringes. Hence, the S/N of the 14 brighter sources could not be improved by using the FD method.

Out of the remaining 25 sources, 11 are fainter than m_K ~3.0. It is found that 9 of those 11 sources were observed in the presence of high speed wind ($>$ 40 km h^{-1}) resulting in telescope oscillations (frequency $<$ 5 Hz). One source (SAO 145698) was observed during daytime when background noise was very high. Another source (SAO 76450) occasionally drifted out of the 10×10 pixel sub-array due to improper telescope tracking at lower elevation. Hence, these 11 fainter sources did not show improvement in S/N due to observational difficulties.

The average enhancement obtained in the value of S/N for 29 sources is 18% after application of the FD method. It is also found that among the 29 sources showing significant improvement in S/N, 19 are fainter than m_K ~3. In fact, the largest improvement in S/N using the FD method is obtained

in the light curve of a faint source, SAO 77271 (m_K ∼3.3). The S/N of the light curve has improved from 32 to 55 (72%). The fainter objects ($m_K > 3.0$) are mainly affected by photon noise from the sky background but have a higher noise content at specific frequencies (31 Hz, 50 Hz, etc) which is removed by using the FD method. That is why they show a good response to the application of the FD method on removing noise at these specific frequencies.

5.1.2 S/N after using the CD method

We now take up S/N improvement obtained using the combination method. It must be noted that in the CD method, FD is applied first, followed by WT. WTs decompose any signal into 'average coefficients' and 'detail coefficients.' It is possible to directly remove fluctuations from the light curve without knowledge of their frequencies by setting suitable cutoffs. That is why it is not surprising that the CD method has shown a significant improvement in S/N in all but five of the light curves (except IRC -10564, RT Cap, IRAS 04320+2519[a], SAO 92755[b] and CW Cnc) and performed better than the FD method. The sources IRC -10564 and CW Cnc were observed at a lower elevation of 16° and 18° respectively. Their light curves are affected by large scintillations. RT Cap was observed in broad daylight and its light curve is affected by large background noise. It was partly cloudy during the observation of IRAS 04320+2519[a] and telescope oscillation added uneven noise to the light curve of SAO 92755[b]. Hence, denoising methods did not yield improvement for these cases.

It is mentioned above that in the CD method, WT is applied after the application of the FD method to the observed light curves. So, the S/N of 29 light curves was already enhanced by an average of 18% using the FD method before application of wavelets. The histogram plot (bottom panel of Fig. 11) shows that 38 sources were below S/N ∼40 before application of any denoising method. The number reduced to 29 by using the FD method which was further reduced to 24 after the application of the WT. The cumulative distribution plot in Figure 12 (short dashed curve) shows that 70% of the Raw light curves fall in the region S/N < 40. The application of the FD method has reduced it to 56% (long dashed curve). Then the application of WTs (in CD) further reduced it to 45% (solid curve). The faintest object in our sample, IRAS 03333+2359, which showed an improvement in S/N from 21 to 24 after application of the FD method, has further shown an improvement in S/N of 32 after the application of the CD method (Fig. 7). One source (SAO 77271) has shown a significant improvement after the application of FD and CD methods. It has shown an improvement in S/N from 32 to 55 after using the FD method which is further improved to 74 after the application of WT in the CD method (Fig. 9).

5.2 Model Fits to Denoised Light Curves

We next consider the possible improvement in the light curves for better model fits to determine the UD values (or UD limit on unresolved sources) after the application of FD and CD methods. To examine this aspect, fits to all three (i.e., Raw, FD and CD) light curves from all the sources have been carried out. The light curves were fitted using the non-linear least squares method. Details on the model fit parameters and analysis can be found in Chandrasekhar & Baug (2010).

Out of the original sample of 54 sources considered for S/N improvement, 50 sources could be used for model fits. The remaining four sources, though bright (m_K <3.0), could not be fitted to a model curve for the following reasons. The light curve of SAO 92755[b] is too noisy to fit due to telescope tracking problems and noise could not be reduced by FD or CD methods. The light curves of TU Gem and VV Cnc suffer from fringe distortions possibly because of the variable rate of the lunar component due to limb irregularities. The light curve of IRC +20177 was observed in a 20×20 pixel sub-array to accommodate its visual binary component. Sampling time in the 20×20 pixel sub-array is poorer than 10×10. Its poor sampling time of ∼14 ms provided a few data points

on the fringes and could not be fitted properly. However its binary separation of 700±50 mas was obtained at a position angle of 109°.

After obtaining the best fit to the light curves, the standard deviation (SD) of the residuals (data − model) has been calculated for (a) the total data set of 200 points (∼1.8 s) used in the model fit and (b) the fringe portion (40 data points with the first fringe of the light curve in the middle). Ideally, values of the SD in the fringe portion ($\mathrm{SD_{fringe}}$) as well as the total data set ($\mathrm{SD_{total}}$) should decrease after the application of denoising methods. We expect this to happen because noise in the observed light curve is generally reduced by the denoising methods. It was indeed found that the $\mathrm{SD_{fringe}}$ and $\mathrm{SD_{total}}$ values for denoised light curves are lower than the Raw data in most of the sources. However, we have introduced one more parameter called $\mathrm{SD_{ratio}}$ ($=^{\mathrm{SD_{fringe}}}/_{\mathrm{SD_{total}}}$) to examine the improvement of the model fit in the fringe region relative to the rest of the light curve. $\mathrm{SD_{ratio}}$ along with $\mathrm{SD_{fringe}}$ and $\mathrm{SD_{total}}$ values for all three cases (Raw, FD and CD) is listed in columns 6–14 of Table 2. The lower the value of $\mathrm{SD_{ratio}}$ is, the better the fit to the fringes is.

5.3 Improvement in Model Fits

When we examine Table 2, in most of cases, $\mathrm{SD_{ratio}}$ for CD is higher than $\mathrm{SD_{ratio}}$ for Raw and FD light curves, which shows that CD light curves give a poor fit to the fringes compared to FD or the Raw light curves. This result arises because the enhancement in S/N seen from the CD method is mainly due to a better denoising effect in the non-fringe region compared to the fringe region. The CD method results in a slight smoothing of the light curves in general and leads to a higher UD value in the model fit. Only in the case of a well-resolved source (TX Psc) is the $\mathrm{SD_{ratio}}$ value for CD lower than the other two. These results are also illustrated in Figure 13. In the figure, $\mathrm{SD_{ratio}}$ values of all three methods are plotted by arranging the $\mathrm{SD_{ratio}}$ values for Raw data in ascending order. It can be seen that while the $\mathrm{SD_{ratio}}$ values for the FD method fluctuate above and below the Raw values, the ratio generally shows higher values for CD than the other two methods.

Out of the 50 sources selected for the model fits, about one third (17) have a lower $\mathrm{SD_{ratio}}$ value for the Raw light curve than that for FD or CD. For half of the sources (24) the $\mathrm{SD_{ratio}}$ is not significantly different between Raw and FD but they are lower than CD (Fig. 13). For the remaining eight sources; namely, BD+26 1131, C* 3246, IRAS 06395+2409, SAO 109252, SAO 75669, HD 249571, NSV 1406 and IRAS 05551+2305, the $\mathrm{SD_{ratio}}$ value for FD is significantly lower than both Raw and CD data. Out of the eight sources, six showed earlier significant S/N improvement when applying the FD method. Those sources are marked in Figure 13 along with their S/N improvement expressed as a percentage. These sources are all fainter than m_K ∼3.3.

5.4 Resolved and Unresolved Sources in the Sample

Out of 50 sources, we find on analysis that five are reported to be resolved sources. Our values agree well with the earlier reported UD angular diameters. They are listed in Table 3 along with the references to their earlier reports in the last column. A close examination of our model fits and details of sources in the literature reveals that two more sources are expected to be resolved. There are two LO observations of UZ Ari (IRC +20052). This source is a semi-regular variable with a period of 163 d. Fits to the two light curves of the source in two different events provide comparable UD values of 5.5±0.5 mas and 6.0±0.5 mas respectively. According to the angular diameter prediction method discussed in Baug & Chandrasekhar (2012), the expected UD value for this source is 4.2±1.0, which is a little lower than the measured values. However, the presence of a circumstellar shell may lead to a higher UD angular diameter at 2.2 μm. The other source, SAO 92697, is also a semi-regular variable with a period of 206 d. A close examination of the model fit reveals that the source is expected to be resolved. These sources are also listed in Table 3.

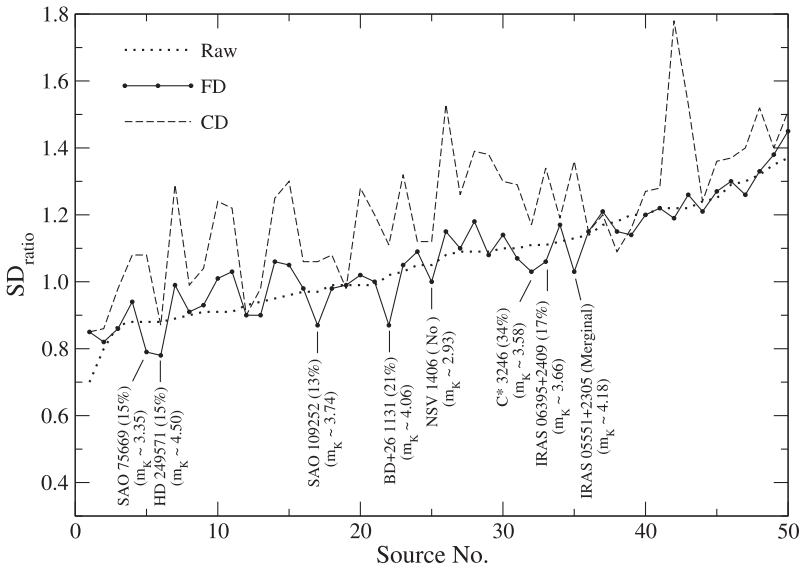

Fig. 13 SD_{ratio} of Raw (*dotted line*), FD (*solid line*) and CD (*dashed line*) light curves are plotted with SD_{ratio} of Raw data arranged in ascending order. The SD_{ratio} values of CD methods are generally higher (indicating a poorer fit to the light curve) than the other two. SD_{ratio} for FD fluctuates with respect to the Raw values. The sources which show the lowest SD_{ratio} values for the FD method (which are the best fit to the light curves) are marked along with their S/N enhancement (in percentage) obtained using the FD method.

In three resolved sources (CW Cnc, RT Cap and UZ Ari[a]), there is no improvement in S/N when using the FD method and hence using Raw data is the best in model fits. In two cases (RS Cap and UZ Ari[b]) SD_{ratio} values for FD are the lowest and hence best fit to the model. In the case of RS Cap, no improvement in S/N has been obtained but the removal of noise frequencies using FD has cleaned the fringes for better fitting. In the case of UZ Ari[b], improvement in S/N using the FD method has been obtained. In two other sources (SAO 118044 and SAO 92697) Raw and FD data give comparable fits though an improvement in S/N is not seen after the application of the FD method. For the important well resolved source, TX Psc, the best fit is obtained by using the CD method.

The light curve and model fits of the remaining sources have been carefully examined to see if any of these sources are resolved. We find that all of these sources are unresolved, but the limit of resolution varies from source to source depending on the S/N and other conditions. The faintest source, IRAS 03333+2359 ($m_K = 5.1$) with an S/N$\sim$24, is best fitted with an FD light curve giving a limit ≤ 4.3 mas. The lowest limit to the resolution of ≤ 3.5 mas is obtained for UY Ari ($m_K = 3.7$). A good improvement in the S/N is obtained by applying the denoising methods on this source and all three light curves are fit to UD limits. For most of the sources with good light curves, we obtained a resolution limit close to ≤ 4.0 mas.

6 CONCLUSIONS

A noise reduction method for LO light curves using FTs and WTs and their combination has been carried out. A total of 54 light curves has been chosen as a sample. We reject the WT alone as it smooths the light curve, which finally leads to fitting an improper angular diameter value. S/N

Table 3 Resolved Sources in the Sample (UD Values)

Source	Filter (μm)	UD Ang. Dia. (mas)	Earlier Reported UD (mas)	Reference
RT Cap	2.20/0.40	8.1±0.3	7.72±0.16 8.18±0.21	White & Feierman (1987) van Belle et al. (2000)
RS Cap	2.37/0.10	7.7±0.5	7.75±0.67 7.70±0.80	Richichi et al. (1992) Dyck et al. (1998)
CW Cnc	2.20/0.40	7.0±0.5	7.05±0.33	White & Feierman (1987)
SAO 118044	2.20/0.40	4.9±0.5	4.85±0.23	White & Feierman (1987)
TX Psc	2.37/0.10	10.6±0.5	7.50 to 11.45	Richichi et al. (2005)
UZ Ari[a]	2.20/0.40	6.0±0.5	—	—
UZ Ari[b]	2.20/0.40	5.5±0.5	—	—
SAO 92697	2.20/0.40	4.7±0.5	—	—

Notes: the sources which have been observed twice are marked with superscripts a and b in the column.

enhancement occurs in both the Fourier and combination methods. The combination method shows good performance in terms of S/N improvement. In a few cases, Fourier denoised light curves, which have a significant improvement in S/N, show the best model fits. For most of the bright sources the Raw data appear to be the best for model fits. It has been noted that the FD method performs better in the fainter regime ($m_K \geq$3.3). For fainter objects ($m_K >$3.3) where background noise dominates, it appears that a better fit is obtained with FD light curves because noises at specific frequencies are filtered out. In the application of the CD method, although there is a substantial improvement in S/N for most of the cases, an averaging effect happens in the light curves. This leads to a larger limit on the fitted UD angular diameter values compared to FD and Raw data. However, in the case of well-resolved sources like TX Psc, where the fit is less affected by smoothing, CD also provides a good fit.

Five sources in our sample are clearly resolved and were reported earlier in the literature. The fitted angular diameters are in good agreement with earlier measurements. From our analysis of light curves, we expect two more sources to be resolved (Table 3). One of these sources (UZ Ari) has been observed twice. There are no earlier reports of angular resolution for these two sources. The rest of the sources in our sample are unresolved. Most of them are expected to have UD values $<$4 mas.

Acknowledgements This work was supported by the Dept of Space, Govt of India. This research made use of the SIMBAD database operated at the CDS, Strasbourg, France and the catalogs associated with it. We thank the referee for valuable suggestions that improved the quality of this paper.

References

Adamakis, S., Eyres, S. P. S., Sarkar, A., & Walsh, R. W. 2011, MNRAS, 414, 2195
Baug, T., & Chandrasekhar, T. 2012, MNRAS, 419, 866
Chandrasekhar, T., & Baug, T. 2010, MNRAS, 408, 1006
Chandrasekhar, T., & Mondal, S. 2001, MNRAS, 322, 356
Cutri, R. M., Skrutskie, M. F., van Dyk, S., et al. 2003, VizieR Online Data Catalog, 2246, 0, Available at: *http://irsa.ipac.caltech.edu/cgi-bin/Gator/nph-dd?catalog=fp_psc*
Dyck, H. M., van Belle, G. T., & Thompson, R. R. 1998, AJ, 116, 981

Fors, O., Richichi, A., Otazu, X., & Núñez, J. 2008, A&A, 480, 297
Kashlinsky, A., Arendt, R. G., Ashby, M. L. N., et al. 2012, ApJ, 753, 63
Kopeikin, S. M., & Potapov, V. A. 2004, MNRAS, 355, 395
Mondal, S., & Chandrasekhar, T. 2002, MNRAS, 334, 143
Polygiannakis, J., Preka-Papadema, P., & Moussas, X. 2003, MNRAS, 343, 725
Richichi, A., di Giacomo, A., Lisi, F., & Calamai, G. 1992, A&A, 265, 535
Richichi, A., Percheron, I., & Khristoforova, M. 2005, A&A, 431, 773, CHARM2: An updated Catalog of High Angular Resolution Measurements, Online available at: *http://vizier.cfa.harvard.edu/viz-bin/VizieR?-source=J/A+A/431/773*
van Belle, G. T., Thompson, R. R., & PTI Collaboration 2000, in American Astronomical Society Meeting Abstracts, Bulletin of the American Astronomical Society, 32, 1476
White, N. M., & Feierman, B. H. 1987, AJ, 94, 751